Automatic Quality Inspection and Intelligent Prevention of Prefabricated Building Construction Based on BIM and Fuzzy Logic

Weini Ma*

1   School of Engineering Economics, Henan Institute of Economics and Trade, Zhengzhou, 450000, China

ARTICLE INFO	ABSTRACT
	The construction industry plays an important role in China's economy. However, traditional construction quality inspection methods have problems such as low efficiency, high leakage rate, and poor real-time performance. Therefore, taking the appearance quality defects of reinforced concrete engineering as an example, this study combines building information models and computer vision technology. By this way, it can achieve automatic quality inspection and intelligent quality problem prevention, to improve the quality management level during the construction process. In this study, ResNet50 network was pre-trained and classified using a self-made defect image database. After transfer learning, the accuracy values of the training and testing sets remained stable at around 0.95 and the loss value remained stable at around 0.10 after 10 epochs, indicating a significant improvement in learning performance. In the defect area quantification experiment, four corner coordinates of the defect image were calculated. These corner coordinates are simultaneously obtained and saved during on-site image acquisition. According to the calculation results, the defect area of honeycomb is approximately 67.67 square centimetres. These results confirm that this method improves the efficiency and accuracy of quality inspection and has potential application in quality inspection of prefabricated building construction.

1. Introduction

Due to the widespread application of digital technology in architecture, prefabricated buildings have gradually become a new architectural model. This construction method has attracted the attention of investors and builders due to its high degree of modularity, environmental protection, efficiency, and controllable quality. In recent years, the promotion and popularization of prefabricated building construction has indeed demonstrated its strong potential in the construction industry. But the rapid expansion of the industry has also brought a series of challenges. Among all the issues, quality management is particularly prominent. Traditional construction quality inspection methods are no longer sufficient to meet the needs of modern construction, as they often have low efficiency and are difficult to detect problems in a timely

---

manner, which directly affects the progress and quality of the project [1]. To address this challenge, experts have proposed new research based on Building Information Modeling (BIM) and Fuzzy Logic (FL). This study delves into the mechanism of Deep Learning (DL), elucidates the types of image segmentation algorithms, and introduces FL. Then, using Computer Vision (CV) technology, the strategy of combining fuzzy reasoning and direct reasoning was studied to achieve intelligent decision-making of construction quality problem prevention and control measures [2]. The overall structure of this study mainly includes four parts. Firstly, the research achievements and shortcomings of BIM and CV in engineering quality automatic inspection at home and abroad were summarized. Secondly, the construction of DL and FL based on BIM was studied and designed. Then, algorithm defect quality results and analysis were conducted through experiments. Finally, these results were summarized, the shortcomings of the research were pointed out, and future research directions were proposed.

2. Related Works

As the construction industry develops and technology advances, prefabricated construction has become a trend of attention and adoption. However, issues such as construction quality control, automatic inspection, and intelligent prevention and control are challenges for prefabricated buildings [3]. Therefore, experts are increasingly studying how to improve engineering quality and efficiency. Porwal et al. used building information models to simulate on-site data during the project lifecycle and analyze the chain reaction of building changes. They established a system dynamic model to map the interactions in the system, and used BIM data to analyze the dynamic behavior of each variable due to changes in the working range. These studies confirm that customers can reduce waste by 25% by planning before the project and collaborating with BIM design work [4]. Mahamood and others improved the seismic building design workflow for Malaysian government projects. Through semi-structured interviews with small samples from both inside and outside government technical institutions, including seven respondents including structural engineers, architects, and relevant consultants, all with over five years of experience in architectural design and construction. These studies evaluated the workflow of seismic resistant building design and found that there are four main factors that need to be improved during the design phase: visual limitations, work changes, data management, and coordination [5]. Arias et al. combined BIM with advanced knowledge representation and reasoning capabilities to unify the capture and fuzzy reasoning of knowledge in various fields. Previous experience has shown that this formal method can be effectively applied in a large number of fields. In addition, by integrating inspection functions in design tools, it can be ensured that the model complies with rules at every step. To validate this method, a preliminary inference engine was implemented using CLP (Q/R) and ASP constraints, and several BIMs were evaluated [6]. Koo et al. aimed to explore the advantages of BIM in preventing design defects during the design phase of construction projects. This study identified key design defect prevention themes through qualitative analysis of 160 leading indicators of design defects. Then, key supporting themes for BIM were identified by matching appropriate BIM functions with each theme. This study identified the necessary data, project stakeholders, operations, and applicable BIM functions to prevent specific design defects [7].

Zou et al. proposed an adaptive content aware low-pass filtering layer that predicts individual filter weights for each spatial position and channel group of input feature maps. The effectiveness and generalization of this method in multiple tasks were studied, including image classification, semantic segmentation, instance segmentation, video instance segmentation, and image to image translation. The qualitative and quantitative results confirm that the proposed method can

effectively adapt to different feature frequencies, avoid aliasing, and retain useful recognition information [8]. Kulkarni et al. proposed a vision based optimized deep neural network for embedded platforms. This model is called QF MobileNet. By addressing redundancy and quantization losses in the existing benchmark MobileNet architecture, inference accuracy and resource utilization can be optimized. Performance validation was conducted on the ImageNet dataset and compared with the benchmark MobileNet architecture. The inference accuracy of the QF-MobileNetV2 floating-point model is 73.36%, and the inference accuracy of the quantitative model is 69.51%. The inference accuracy of the MobileNetV3 floating-point model is 68.75%, and the inference accuracy of the quantitative model is 67.5% [9]. The research goal of Jain is to develop a feature based algorithm for two-dimensional part recognition in intensity images. Industrial vision systems are usually only suitable for specific applications, so it is necessary to study object recognition and classification issues. RGB images and Fourier descriptor technology were used for object recognition, and different networks were used for processing. These studies confirm that network structure, learning rate, and momentum have an impact on classification accuracy [10]. Han et al. proposed a multi-level network architecture for the study of multi view stereo sequences in DL. This method aims to improve the accuracy of depth prediction while addressing the issues of noisy images and computational resources. Firstly, 2D feature map is converted into a 3D cost volume, while processing pixel and depth information. These experiments confirm that this method achieves better results in denoising and deep inference than existing methods, and shows robustness to noisy images [11]. Duan and Liu proposed a method to measure and optimize stress parameters of prefabricated buildings by using BIM technology. The method constructs BIM engineering library and subdivides BIM units, and uses nonlinear iterative method to complete the 3D model reconstruction of structural design. Then, the stress parameters are measured and analyzed to optimize the construction parameters. The simulation results show that the reliability of this method is over 90%, the stability is high, and the performance is excellent [12]. Yuan proposed a BIM based whole-process building cycle control method. The periodic control constraint model is established for parameter analysis, and BIM technology is used to realize parameter fusion and control convergence judgment. Use BIM scheduling to build a resource scheduling model and effectively manage the process cycle. The experimental results show that the method has good convergence, small control error, safety quality error is less than 0.01, and strong cycle control ability [13]. Chen et al. proposed a new computational method for BIM alignment of aerial photos, detection and reconstruction of concrete defects by binding registration algorithm. This method uses the material semantics in BIM to locate the defect area, correct the aerial image attitude, and improve the reconstruction accuracy. Experiments show that the error rate is reduced to 56.8%, the intersection ratio is increased by 6.4%, and the defect shape can be accurately reconstructed in three-dimensional space, which is suitable for urban transformation and intelligent applications [14]. Levine et al. proposed a BIM-based automatic inspection framework that uses deep learning for semantic segmentation and identification of damage in images, and correlates damage with building components in BIM. The damage state of the component is classified according to the vulnerability model and combined with the structural analysis. The framework was tested in a simulated building model, demonstrating a high-precision damage state assignment that can be used for performance-based seismic building safety assessment [15].

In summary, although there have been in-depth studies in the field of building quality management, the methods of using information technology to achieve automated and intelligent quality inspection are still scarce in the existing literature. The existing methods often ignore the acquisition and analysis of the deep-level information of quality problems, and lack the means to

effectively integrate building data and image recognition technology, which makes the prediction and prevention of quality problems limited in practical operation. To address these shortcomings, a new model combining building information model and advanced computer vision technology is proposed in this study, which makes up for the shortcomings of traditional methods in automatically identifying and locating building quality defects. This research not only improves the accuracy and efficiency of the inspection, but also provides a new and widely applicable quality management tool for the construction industry, which is expected to promote the progress of quality control methods in the industry.

3. Algorithm for Automatic Acquisition of Construction Quality based on BIM and FL

This study first elaborated on DL, followed by the classification and FL of image segmentation algorithms. Then, through DL and FL, the knowledge required for decision-making is transformed into semantic information that can be understood by computers. Combined with fuzzy reasoning and direct reasoning methods, the decision-making of prevention and control measures for construction quality problems is achieved.

3.1 DL based Fuzzy Logic Construction

FL can be used as a part of DL to help models better handle uncertainty and ambiguity. Convolutional Neural Network (CNN) is one of the most important models in DL, playing a significant role in promoting the development of image classification, recognition, and understanding technologies. It adopts convolutional kernel weight sharing mode, reduces network model parameters, achieves deep network structure, obtains more abstract and deep level features, and accelerates model training speed [16, 17]. Figure 1 shows the main structure of CNN.

x	H_1	H_2	H_3	H_4	$H_4 \sim H_R$
Input layer	Convolution layer	Pooled horizon	Convolution layer	Pooled horizon	Pooled horizon
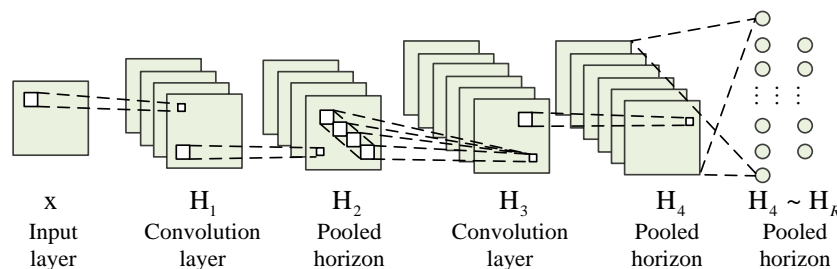
Fig. 1. The structure of CNN

In Figure 1, the input layer preprocesses the raw data, including normalization, dimensionality reduction, and decorrelation operations. The convolutional layer is the core of CNN, which applies convolutional kernels to the input data for convolution operations, and then performs nonlinear mapping through activation functions to generate feature maps as output [18]. Formula (1) is a convolutional operation.

$$S(i, j) = (X * K)(x, j) = \sum_h \sum_n x(i+h, j+n)k(h,n) \tag{1}$$

In Formula (1), $S(i, j)$ represents the convolution result. X represents a two-dimensional input image. $*$ represents convolution operation. K represents the corresponding two-dimensional convolutional kernel. $x(i+h, j+n)k(h,n)$ represents the image unit of row $i+h$ and column $j+n$. $k(h,n)$ represents convolutional kernel unit. Figure 2 shows the specific convolution operation.

Characteristic map   Convolution kernel   Convolution result
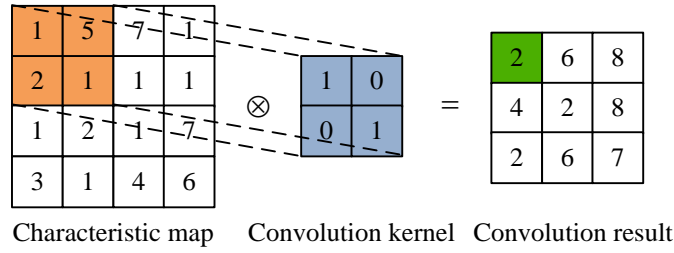
Fig. 2. Convolution schematic

In Figure 2, the step size of convolution operation is 1, and the convolution kernel is 3 × 3. Usually, convolution operations include VALID and SAME. Among them, VALID is achieved by convolving the size of the image without filling the edges. SAME fills image edges by the size of convolutional kernels. Formula (2) is the calculation for VALID.

$$w_{out} = \frac{w - F}{s} + 1$$
$$h_{out} = \frac{h - F}{s} + 1$$

(2)

In Formula (2), w and h represent the input image resolutions. w_{out} and h_{out} represent the output image resolutions. s represents the step size. Formula (3) is the calculation of SAME.

$$w_{out} = \frac{w + 2p - F}{s} + 1$$
$$h_{out} = \frac{h + 2p - F}{s} + 1$$

(3)

In Formula (3), p represents the size of the filled image boundary. CNN often contains multiple convolutional layers. To avoid training difficulties caused by too many parameters, it is necessary to perform pooling operations after the convolutional layer. Common pooling rules include maximum pooling and average pooling. The fully connected layer is usually located at the end of the hidden layer, and the 3D feature map is expanded into a one-dimensional vector. Normally, the fully connected layer uses ReLU activation function in Formula (4).

$$\mathrm{Re}\, LU(x) = \max(O, x)$$

(4)

DL and FL can be used in combination. For example, FL can be used to preprocess data, and then DL model can be used for further analysis and decision-making. In daily life, many concepts cannot be described in deterministic language, such as more or less, height or short, youth or old age, all of which have ambiguity. FL can solve these ambiguity problems. It does not directly classify propositions as true or false, but rather refers to propositions as "partial truth." The degree of belonging, whether true or false, can be measured by membership, with membership values ranging from 0 to 1 [19, 20]. FL is very important in artificial intelligence, and Figure 3 shows its basic structure.
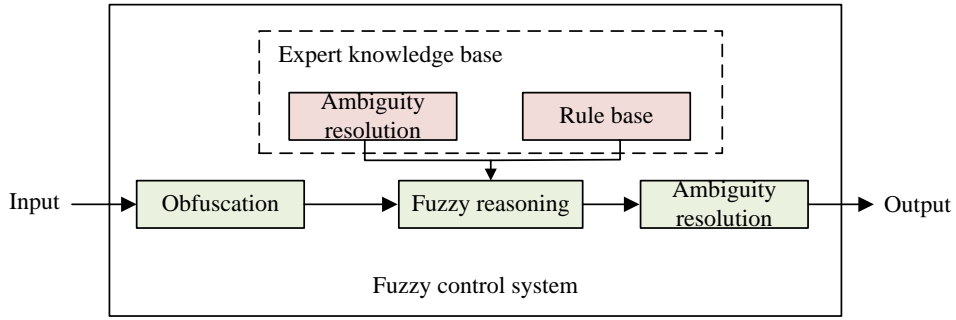
Fig. 3. Fuzzy control system structure diagram

In Figure 3, in the fuzzy control system, the input data need to be fuzzified. The knowledge base is its core, including expert knowledge base and fuzzy rule base. Fuzzy inference generates real-time fuzzy decision results based on input data and fuzzy control rules. The rule of fuzzy reasoning is to use the method of likelihood reasoning for reasoning. Formula (5) sets two fuzzy inference rules.

$$\overline{R}_1 : \quad if \quad \overline{A}_1 \quad and \quad \overline{B}_1 \quad then \quad \overline{C}_1$$
$$\overline{R}_2 : \quad if \quad \overline{A}_2 \quad and \quad \overline{B}_2 \quad then \quad \overline{C}_2 \tag{5}$$

In Formula (5), *if* represents the premise part. *then* represents the conclusion section. $\overline{A}_i$ is a fuzzy subset on the domain U. $\overline{B}_i$ is a fuzzy subset on the domain V. Formula (6) indicates that the new input adopts a fuzzy single point set.

$$\overline{A}' = \frac{1}{x_0}$$
$$\overline{B}' = \frac{1}{y_0} \tag{6}$$

In Formula (6), $\overline{A}$ and $\overline{B}$ are fuzzy sets on the domains x and y, respectively. $\overline{A}$ is the fuzzy subset on the error signal. $\overline{B}$ is the fuzzy subset on the rate of error change. $\overline{C}'$ is the fuzzy subset on the output in Formula (7).

$$\overline{C}' = \bigcup_{i=1}^{2} \overline{C}'_i \tag{7}$$

In fuzzy controllers, fuzzy control rules are represented by logical fuzzy conditional reasoning statements. These statements use a set of fuzzy vocabulary to describe the state changes of input and output variables, such as "large,""medium", and "small." To consider the duality of things and the symmetry of judgments, "positive" and "negative" can be added to represent both situations, and the zero state of the variable can be added. Therefore, Formula (8) represents the fuzzy language word set of input and output variables.

$$\{NB, NM, NS, ZO, PS, PM, PB\} \tag{8}$$

In Formula (8), N = Negative, B = Big, M = Middle, S = Small, ZO = Zero, and P = Positive. When designing a fuzzy controller, there should be a boundary range between the actual input and output quantities, which is called the basic universe, meaning the precise input quantity of fuzzy controller. The membership function can be regarded as a fuzzy domain. The fuzzy domain divided by precise input quantity is called quantization factor. And the output of fuzzy control can be transformed into the basic domain by multiplying it by the scaling factor, and Formula (9) can be obtained.

$$\text{Quantization factor} = \frac{\text{Fuzzy domain}}{\text{Exact input}}$$

$$\text{Exact input} = \frac{\text{Control force precision}}{\text{Fuzzy domain}}$$

(9)

According to the previous fuzzy control rules, fuzzy inference yields a membership function or fuzzy set. The commonly used methods currently include the maximum membership function, the center of gravity, and the weighted average methods. The maximum membership function corresponds to different membership degrees for each fuzzy inference result, and the maximum value can be directly selected as the output value in Formula (10).

$$u_0 = \max \mu_A(u), u \in U \tag{10}$$

If there are multiple output values corresponding to the maximum membership degree in the inference result, the average of these values can be taken as the final output in Formula (11).

$$u_0 = \frac{1}{J}\sum_{j=1}^{J} u_j, u_j = \max_{u \in U}(\mu_A(u)); J = |\{u\}| \tag{11}$$

In Formula (11), J represents the number of outputs with the maximum membership value. The second method selects the center of gravity of the area enclosed by the curve of the membership function and the abscissa as the output value of fuzzy inference. Formula (12) is a continuous equation.

$$u_0 = \frac{\int_U u\mu_A(u)du}{\int_U \mu_A(u)du} \tag{12}$$

When the neighborhood is discrete, it is represented by Formula (13). m represents the stage number of output quantization.

$$u_0 = \frac{\int_U u_k\mu_A(u_k)}{\sum_{k=1}^{m} \mu_A(u_k)} \tag{13}$$

Compared to the maximum membership method, the output inference of the center of gravity method is smoother. Even if there is a slight change in the output signal, its final calculation result usually changes accordingly.

$$u_0 = \frac{\sum_{i=1}^{m} u_i k_i}{\sum_{i=1}^{m} k_i} \tag{14}$$

Formula (14) is the weighted average method. u_i represents the weight coefficient, which should be determined based on the actual situation. When k_i takes $\mu_A(u_i)$, that is, when its membership function value is taken, it is converted to the center of gravity method.

3.2 CV based BIM Construction Quality Automatic Inspection Algorithm

In construction projects, the content of construction quality inspection is numerous and complex, with a large amount of data. And overlapping between different construction tasks may mask quality issues in the previous tasks, leading to ineffective inspections. To improve inspection efficiency and accuracy, it is crucial to automatically generate construction quality inspection plans. This plan is based on quality standard specifications and progress plans, including modules such as inspection tasks, execution time, and inspection points. When generating plans automatically, it is necessary to obtain tasks and executable time based on standard specifications and progress plans,

reasonably divide inspection batches, and select appropriate checkpoints. Figure 4 shows the specific process.
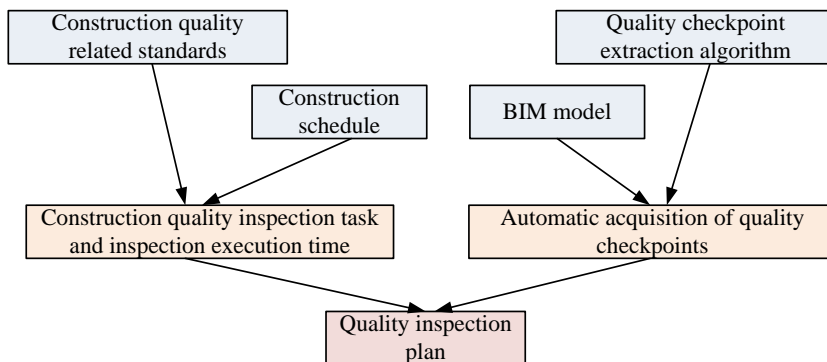
Fig. 4. Automatic generation process of construction quality inspection plan

BIM not only includes specific components such as columns, beams, slabs, etc., but also abstract concepts such as floors and construction sections. In construction quality acceptance, inspection batches are usually divided based on abstract concepts, which becomes the foundation and core of quality management. Therefore, a method for automatically generating construction quality checkpoints based on BIM data was proposed. This method starts from the inspection batch and explores the association of national standards with BIM data to achieve automatic extraction of quality inspection points. The detailed algorithm can be referred to Figure 5.
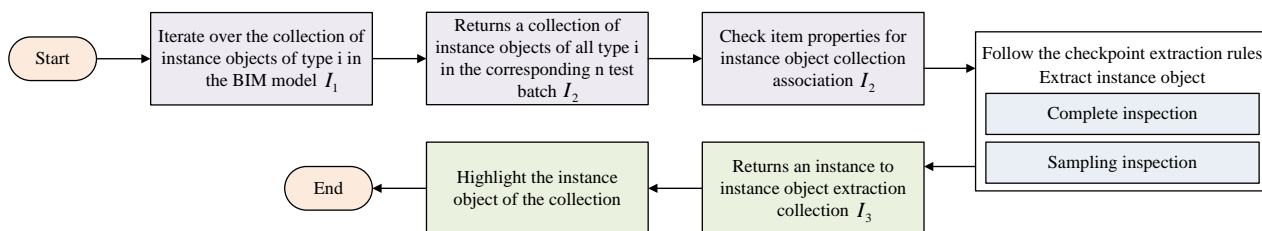
Fig. 5. Quality automatic check algorithm flow chart

DL is important in image classification, object detection, and segmentation. Image classification takes relatively less time, and object detection and segmentation require preprocessing. In construction, traditional CV methods can quantify simple appearance quality defects. Therefore, this study uses image classification methods for automatic recognition of defect types and quantifies defect features using traditional methods. Compared with object detection and segmentation, this method can achieve the same results without labeling the dataset, achieving rapid defect type recognition and quantification. Figure 6 shows the automatic inspection process for construction quality based on CV.
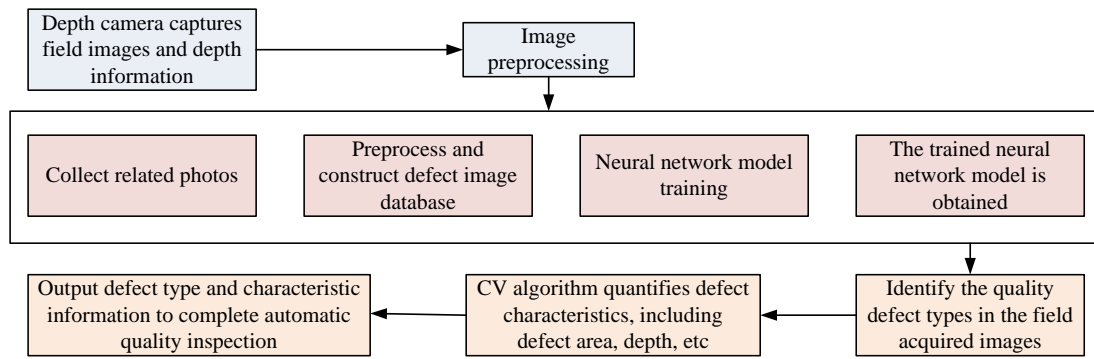
Fig. 6. Flow chart of automatic inspection of construction quality based on CV

Transfer learning is a strategy in machine learning that utilizes knowledge from other fields to solve current limited information problems. This method first trains on the original dataset, and then fine tunes the application to the target dataset, effectively reducing the demand for big data and high-end hardware, while saving time and manpower. In CV, utilizing deeper CNN and transfer learning can extract higher-level features, thereby improving image classification performance. But as the depth of network increases, the disappearance of gradients becomes a problem, affecting training efficiency [21, 22]. To solve this problem, ResNet was proposed. ResNet preserves a large amount of gradient information in the first few layers through residual mapping. The residual block learns residual mapping and adds the mapping learned from the original network to the input. Compared to direct mapping, residual mapping is more convenient. In addition, residual units increase sensitivity to small changes in local features, further adjusting network weights, and improving training performance. Due to its few parameters and superior performance, ResNet has been widely used in DL in recent years [23, 24] (see Figure 7).
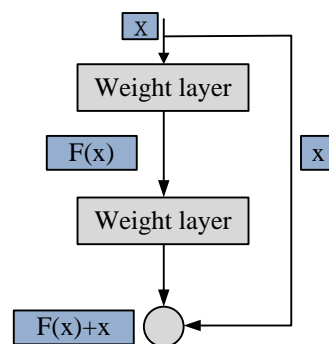
Fig. 7. Residual learning unit

ResNet networks have different layers of structure, including 18, 34, 50, and 101, with ResNet50 and ResNet101 being the most commonly used types. Although ResNet101 is relatively deep, the number of parameters is twice that of ResNet50. Therefore, ResNet50 was chosen as the main algorithm for identifying quality defect types. Table 1 shows the specific structure.

Table 1
ResNet five deep network structures

Name	The 18th	The 34th	The 50th	The 101th
Conv1 /	7 * 7, 64, step 2	3 * 3 Maximum pooling, step 2		
Conv2	$\begin{bmatrix} 3*3,64 \\ 3*3,64 \end{bmatrix}*2$	$\begin{bmatrix} 3*3,64 \\ 3*3,64 \end{bmatrix}*3$	$\begin{bmatrix} 1*1,64 \\ 3*3,64 \\ 1*1,256 \end{bmatrix}*3$	$\begin{bmatrix} 1*1,64 \\ 3*3,64 \\ 1*1,256 \end{bmatrix}*3$
Conv3	$\begin{bmatrix} 3*3,128 \\ 3*3,128 \end{bmatrix}*2$	$\begin{bmatrix} 3*3,128 \\ 3*3,128 \end{bmatrix}*4$	$\begin{bmatrix} 1*1,128 \\ 3*3,128 \\ 1*1,512 \end{bmatrix}*4$	$\begin{bmatrix} 1*1,128 \\ 3*3,128 \\ 1*1,512 \end{bmatrix}*4$
Conv4	$\begin{bmatrix} 3*3,256 \\ 3*3,256 \end{bmatrix}*2$	$\begin{bmatrix} 3*3,256 \\ 3*3,256 \end{bmatrix}*6$	$\begin{bmatrix} 1*1,256 \\ 3*3,256 \\ 1*1,1024 \end{bmatrix}*6$	$\begin{bmatrix} 1*1,256 \\ 3*3,256 \\ 1*1,1024 \end{bmatrix}*23$
Conv5	$\begin{bmatrix} 3*3,512 \\ 3*3,512 \end{bmatrix}*2$	$\begin{bmatrix} 3*3,512 \\ 3*3,512 \end{bmatrix}*3$	$\begin{bmatrix} 1*1,512 \\ 3*3,512 \\ 1*1,2048 \end{bmatrix}*3$	$\begin{bmatrix} 1*1,512 \\ 3*3,512 \\ 1*1,2048 \end{bmatrix}*3$
/	Average pooling, 100-d fc, softmax			
Parameter	$1.8*10^9$	$3.6*10^9$	$3.8*10^9$	$7.6*10^9$

4. Experimental Results and Analysis Based on BIM and FL

To verify the experimental effectiveness of defect quantification and fuzzification processing, this study first used deep transfer learning to train the model to enhance its recognition accuracy and practical application effectiveness. Subsequently, honeycomb images were selected for quantitative research on defect features, and the area of defects was estimated to demonstrate the practicality of automatic inspection. Finally, different types of defect quantification information were fuzzified to further ensure the effectiveness of decision-making.

4.1 Analysis of Model Training and Deep Transfer Learning

The goal of this experiment is to construct an image database containing seven types of defects, including honeycomb, pitted surface, exposed tendon, hole, crack, water seepage, and normal, for training neural network models. To enhance the generalization ability and robustness of the model, it is necessary to collect a large amount of annotated sample data for neural network learning. Due to the lack of readily available public datasets for these seven defects, it is necessary to obtain sufficient defect images and construct appropriate datasets through on-site collection and online search. Cracks and normal images were obtained from SDNET2018 dataset and cropped into images of 300 * 300 pixels. Table 2 shows the final constructed database.

This experiment randomly divided the images in the above database into a training set and a testing set, with a ratio of 8:2, and trained ResNet50 using 100 epochs. Figure 8 shows the training results. Throughout the entire training, the accuracy and loss values of the training and testing sets fluctuated greatly, exhibiting a very unstable training effect. This may be due to the relatively small number of samples in the defect image database and the inclusion of multiple classifications.

Table 2
Defect image database

Image type	Quantity
Honeycomb	108
Pitted surface	100
Exposed bar	101
Opening	45
Water seepage	105
Crack	100
Normal	105
Total	664

(a) ResNet original training accuracy results   (b) ResNet original training loss value results
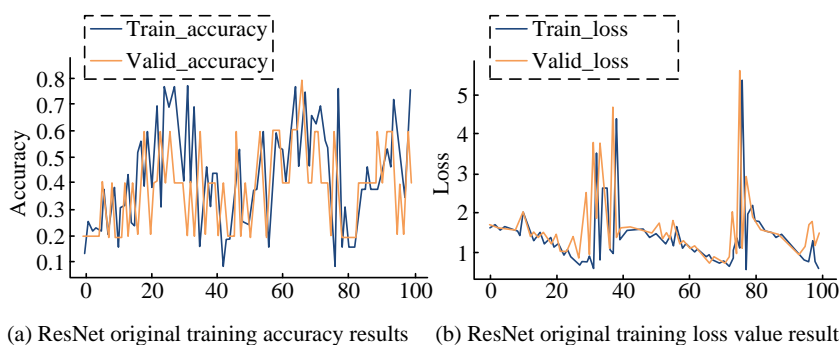
Fig. 8. ResNet50 original training results

To solve the problem of insufficient sample size and high classification, transfer learning methods were used to improve model training and improve its accuracy and effectiveness. Transfer learning utilizes network structures and weights in other fields to handle generalization problems, particularly suitable for small sample recognition. It helps CNN to learn image features by sharing low-level knowledge. Even with limited data volume and computing power, transfer learning can still be effectively applied. The open-source Kaggle cat and dog dataset was used to pre-train ResNet50 network model, and a self-made defect image database was used for classification training. Figure 9 shows the final training results obtained. After transfer learning, the accuracy values of training and testing sets remained stable at around 0.95 after 10 epochs, and the loss value also remained stable at around 0.10, indicating a significant improvement in learning effectiveness.

(a) ResNet original training accuracy results   (b) ResNet original training loss value results
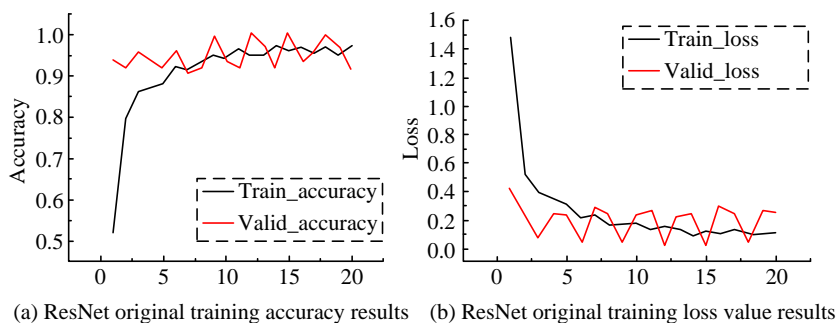
Fig. 9. Training results of ResNet50 after transfer learning

4.2 Quantitative Experiment on Defect Area

This experiment selected images of the honeycomb from the database to further quantify the evolution of defect features in Figure 10(a). Firstly, through statistical analysis of pixels, the specific distribution of RGB pixels was obtained in Figure 10(b). After analysis, the current RGB values of pixels are mainly concentrated within the range of [125, 200]. Taking into account the characteristics of defects in concrete engineering, common defect areas are usually darker in color than normal areas. Therefore, the pixel positions within the RGB value range of [0, 125] are mainly concentrated in the defective part. This interval provides data support for subsequent threshold segmentation.

(a) Honeycomb   (b) Pixel statistical map
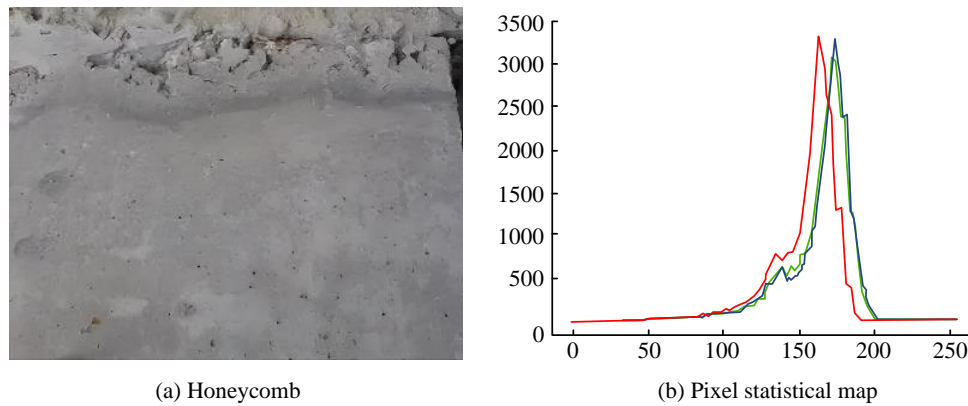
Fig. 10. Cellular pixel statistics

Next, based on the binarization results of the image, the defect threshold interval [0, 125] is used for linear threshold segmentation in this study to enhance image features. Then, through the operation of median filtering, noise is removed to obtain the final threshold segmentation image. Figure 11 shows the specific generation process. In this image, from left to right are the binary images obtained from the original image after graying, the results of enhanced image features, and the denoised images.

(a) Binary image   (b) After enhancing the image features   (c) The image after noise removal
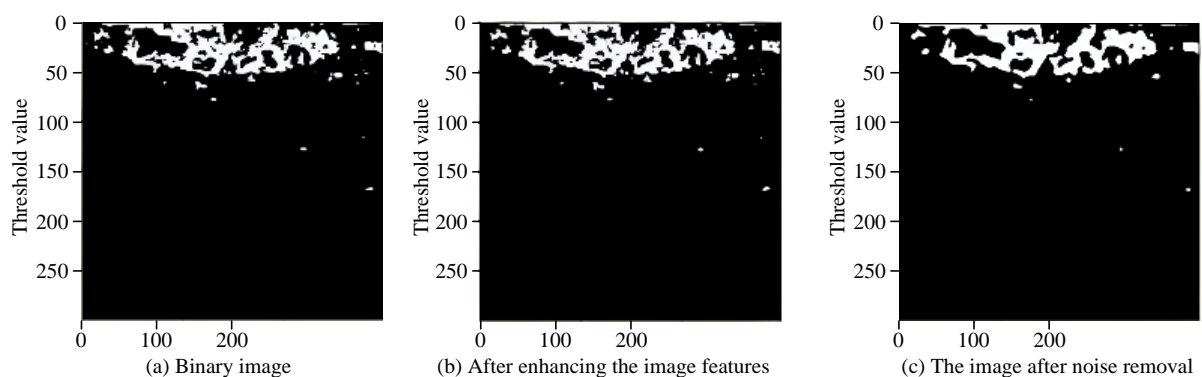
Fig. 11. The generating process of cellular threshold segmentation image

Finally, in the study, the contour of the defective part in the threshold segmentation image was extracted, and the pixel area of the defective part was calculated. To calculate the actual area of the entire image, this study calculated the coordinates of these four corner points of this image,

which were simultaneously obtained and saved during on-site image collection. According to the calculation results, the defect area of the honeycomb is approximately 67.67 square centimeters.

4.2 Intelligent Decision-Making for Prevention and Control of Construction Quality Issues

In the manual for the prevention and control of common engineering quality problems, the description of appearance quality defects is often unclear, and the judgment conditions are not clear enough. Some words such as "small honeycomb," "larger honeycomb," and "deeper honeycomb" can easily cause controversy. To address this issue, this study combines direct reasoning and fuzzy reasoning to construct a reasoning engine for intelligent decision-making of construction quality issues. The input data include the type of defect, BIM information of component, and quantitative information of defect. Defect quantification information needs to be fuzzified by combining the opinions of experts and experienced staff. To ensure the effectiveness and professionalism of fuzzification, expert opinions were referred to and the quantitative information of different types of defects was fuzzified. In addition, the fuzzy set of honeycomb area has also been defined to better express the meanings of "small honeycomb," "larger honeycomb," and "deeper honeycomb." Table 3 provides detailed information.

Table 3
The definition of fuzzy set of cellular quantization index

Discriminator	Specific definition
Alveolus	The proportion of honeycomb area within 20 * 20 square centimeters is less than 4%
Larger cell	The proportion of honeycomb area within 20 * 20 square centimeters is greater than 4%
Shallower cell	The depth is less than or equal to the thickness of the reinforcement protective layer of the member
Deep honeycomb	The depth is greater than the thickness of the steel protective layer of the member

Based on the definition criteria in Table 3, a small honeycomb is defined as a honeycomb area within 20 * 20 square centimeters accounting for 4% or less. Larger honeycombs are greater than 4%. The shallower honeycomb is the thickness of the steel reinforcement protective layer of the component, which is less than or equal to 0.8 D in depth. The deeper honeycomb is greater than 1.2 D. The membership function of the honeycomb quantification index is established in Figure 12. Red represents a small honeycomb. Deep red indicates a larger honeycomb. Light blue indicates a lighter honeycomb. Blue indicates a deeper honeycomb.
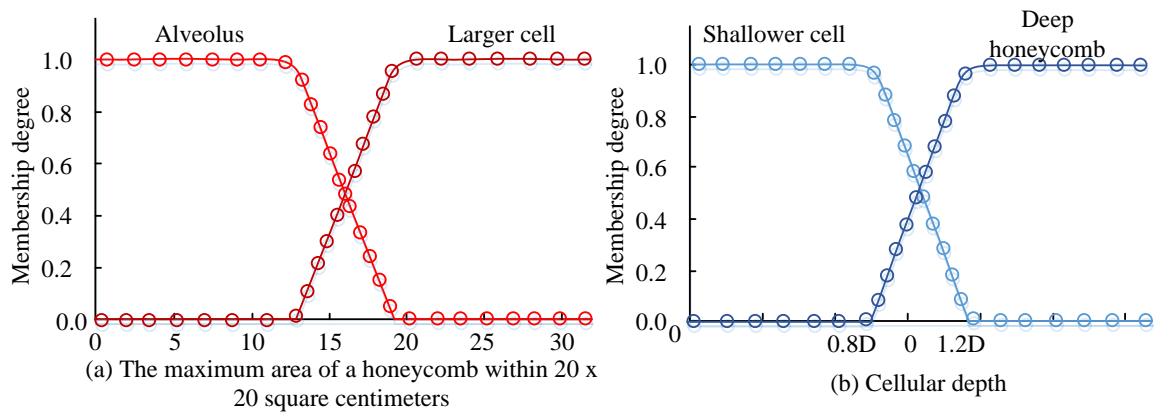
Fig. 12. Fuzzy representation of cellular quantitative index

5. Conclusion

Due to the increasing demand for environmental protection and building quality, prefabricated building construction methods have received increasing attention. Despite the current advancements, challenges persist, such as the timeliness of construction quality assessments, the degree of automation, and the sophistication of decision-making processes. Addressing these issues, this study successfully integrates BIM with the nuanced analytical capabilities of deep learning and fuzzy logic within computer vision to facilitate automatic inspection and intelligent decision-making for construction quality control. This approach has effectively enhanced the quality management processes throughout construction. In the practical application of this study, ResNet50 was pre-trained and further refined with a bespoke defect image database to improve classification training. The results showed that after transfer learning, both the training and testing sets stabilized at a high accuracy rate of around 0.95, and the loss value consistently hovered around 0.10 after 10 epochs. This consistency signifies a notable enhancement in the model's learning performance. Furthermore, in quantifying defect areas, the model accurately calculates and saves the four corner coordinates of defect images, concurrently with on-site image acquisition. One of the practical outcomes observed was the precise measurement of a honeycomb defect area, estimated at about 67.67 square centimeters, underscoring the method's improved inspection efficiency and accuracy. Although this study has made strides in ameliorating the limitations inherent in current construction quality management, the exploration of some issues has been constrained by time and the breadth of knowledge available. For future research directions, there is a substantial scope to build on this groundwork. Anticipated advancements could involve the development of more sophisticated backend algorithms to enhance the model's predictive and analytical capabilities. Additionally, efforts could be made to design user-friendly front-end interfaces, which would make the system more accessible to practitioners in the field. The integration of a broader range of quality metrics and real-time data analysis could also be explored to create a more dynamic and responsive quality management system. Further, there is an opportunity to incorporate augmented reality (AR) technologies to visualize defects and quality measures on-site, providing an immersive and interactive experience for quality inspectors. The convergence of IoT devices could be another avenue, enabling a seamless flow of data from construction sites to the model, facilitating instantaneous updates and decision-making. Lastly, research could delve into the application of this model across different climates and construction styles, ensuring its robustness and adaptability to a diverse range of building environments.

Funding
This research received no external funding.

Data Availability Statement
The datasets generated or analyzed during this study are available from the corresponding author on reasonable request.

Conflicts of Interest
The authors declare that they have no known competing financial interests or personal relationships that could have appeared to influence the work reported in this paper.

Acknowledgement
This research was not funded by any grant.

References

[1] Fini, A. A. F., Maghrebi, M., Forsythe, P. J., & Waller, T. S. (2021). Using existing site surveillance cameras to automatically measure the installation speed in prefabricated timber construction. *Engineering Construction and Architectural Management*, 29(2), 573-600. https://doi.org/10.1108/ECAM-04-2020-0281

[2] Lee, P. C., Lo, T. P., Wen, I. J., & Xie, L. (2022). The establishment of BIM-embedded knowledge-sharing platform and its learning community model: A case of prefabricated building design. *Computer Applications in Engineering Education*, 30(3), 863-875. https://doi.org/10.1002/cae.22490

[3] Yuan, Y., Ye, S., & Lin, L. (2021). Process monitoring with support of IoT in prefabricated building construction. *Sensors and Materials: An International Journal on Sensor Technology*, 33(4), 1167-1185. https://doi.org/10.18494/SAM.2021.3003

[4] Porwal, A., Parsamehr, M., Szostopal, D., & Ruparathna, R. (2023). The integration of building information modeling (BIM) and system dynamic modeling to minimize construction waste generation from change orders. *The International Journal of construction Management*, 23(1/3), 156-166. https://doi.org/10.1080/15623599.2020.1854930

[5] Mahamood, S. Z. H., & Fathi, M. S. (2022). Seismic building design work process using building information modeling (BUM) technology for malaysian government projects. *International Journal of Disaster Resilience in the Built Environment*, 13(2), 211-232. https://doi.org/10.1108/IJDRBE-10-2021-0135

[6] Arias, J., Trm, S., Carro, M., & Gupta, G. (2022). Building information modeling using constraint logic programming. *Theory and Practice of Logic Programming*, 22(5), 723-738. https://doi.org/10.1017/S1471068422000138

[7] Koo, H. J., & O'Connor, J. T. (2022). Building information modeling as a tool for prevention of design defects. *Construction Innovation: Information, Process, Management*, 22(4), 870-890. https://doi.org/10.1108/CI-02-2021-0033

[8] Zou, X., Xiao, F., Yu, Z., Li, Y., & Lee, Y. (2023). Delving deeper into anti-aliasing in ConvNets. *International Journal of Computer Vision*, 131(1), 67-81. https://doi.org/10.48550/arXiv.2008.09604

[9] Kulkarni, U., Meena, S. M., & Gurlahosur, S. V. (2021). Quantization friendly mobileNet (QF-MobileNet) architecture for vision based applications on embedded platforms. *Neural Networks*, 136, 28-39. https://doi.org/10.1016/j.neunet.2020.12.022

[10] Jain, T. (2022). Industrial objects recognition in intelligent manufacturing for computer vision. *International Journal of Intelligent Unmanned Systems*, 10(4), 115-129. https://doi.org/10.1108/IJIUS-04-2020-0004

[11] Han, J., Chen, X., & Zhang, Y. (2022). DEMVSNet: Denoising and depth inference for unstructured multi-view stereo on noised images. *IET Computer Vision*, 16(7), 570-580. https://doi.org/10.1049/cvi2.12102

[12] Duan, Y., & Liu, H. (2023). Research on BIM technology-based measurement method of stress parameters of prefabricated building engineering. International Journal of Critical Infrastructure, 19(3), 199-210. https://doi.org/10.1504/IJCIS.2023.130911

[13] Yuan, X. (2023). BIM-based cycle control method for the whole process of building production and construction. International Journal of Critical Infrastructure, 19(2), 95-107. https://doi.org/10.1504/IJCIS.2023.130447

[14] Chen, J., Lu, W., & Lou, J. (2023). Automatic concrete defect detection and reconstruction by aligning aerial images onto semantic-rich building information model. Computer-Aided Civil and Infrastructure Engineering, 38(8), 1079-1098. https://doi.org/10.1111/mice.12928

[15] Levine, N. M., Narazaki, Y., & Spencer, B. F. (2023). Development of a building information model-guided post-earthquake building inspection framework using 3D synthetic environments. Earthquake Engineering and Engineering Vibration, 22(2), 279-307. https://doi.org/10.1007/s11803-023-2167-y

[16] Wang, X., Cheng, M., Eaton, J., & Hsieh, C. J. (2022). Fake node attacks on graph convolutional networks. *Journal of Computational and Cognitive Engineering*, 1(4), 165-173. https://doi.org/10.47852/bonviewJCCE2202321

[17] Nimrah, S., & Saifullah, S. (2022). Context-free word importance scores for attacking neural networks. *Journal of Computational and Cognitive Engineering*, 1(4), 187-192. https://doi.org/10.47852/bonviewJCCE2202406

[18] Debnath, S. (2022). Fuzzy Quadri partitioned neutrosophic soft matrix theory and its decision-making approach. *Journal of Computational and Cognitive Engineering*, 1(2), 88-93. https://doi.org/10.47852/bonviewJCCE19522514205514

[19] Dey, P., & Jana, D. K. (2022). Evaluation of the convincing ability through presentation skills of pre-service management wizards using AI via T2 linguistic fuzzy logic. *Journal of Computational and Cognitive Engineering*, 2(2), 133-142. https://doi.org/10.47852/bonviewJCCE2202158

[20] Waziri, T. A., & Ibrahim, A. (2023).Discrete fix up limit model of a device unit. *Journal of Computational and Cognitive Engineering*, 2(2), 163-167. https://doi.org/10.47852/bonviewJCCE2202166

[21] Song, D., Lu, T., & Jeudy, J. (2022). Improving sensitivity of arterial spin labeling perfusion MRI in Alzheimer's disease using transfer learning of deep learning-based ASL denoising. *Journal of Magnetic Resonance Imaging*, 55(6), 1710-1722. https://doi.org/10.1002/jmri.27984

[22] Debicha, I., Bauwens, R., Debatty, T., Kenaza, T., & Mees, W. (2023). TAD: Transfer learning-based multi-adversarial detection of evasion attacks against network intrusion detection systems. *Future Generations Computer Systems: FGCS*, 138, 185-197. https://doi.org/10.1016/j.future.2022.08.011

[23] Singh, D., Shukla, A., & Sajwan, M. (2021). Deep transfer learning framework for the identification of malicious activities to combat cyberattack. *Future Generation Computer Systems*, 125, 687-697. https://doi.org/10.1016/j.future.2021.07.015

[24] Elghany, S. A., Ibraheem, M. R., Alruwaili, M., & Elmogy, M. (2021). Diagnosis of various skin cancer lesions based on fine-tuned ResNet50 deep network. *Computers, Materials, and Continuum*, 68(1), 117-135. https://doi.org/10.32604/CMC.2021.016102